ORIGINAL ARTICLE

Correct Laminar Positioning in the Neocortex Influences Proper Dendritic and Synaptic Development

Fanny Sandrine Martineau ⓘ [1], Surajit Sahu[1], Vanessa Plantier[1], Emmanuelle Buhler[1], Fabienne Schaller[1], Lauriane Fournier[1], Geneviève Chazal[1], Hiroshi Kawasaki[2], Alfonso Represa ⓘ [1], Françoise Watrin ⓘ [1] and Jean-Bernard Manent ⓘ [1]

[1]INMED, Aix-Marseille University, INSERM U901, Marseille 13009, France and [2]Department of Medical Neuroscience, Graduate School of Medical Sciences, Kanazawa University, Ishikawa 920-8640, Japan

Address correspondence to Jean-Bernard Manent. Email: jean-bernard.manent@inserm.fr ⓘ orcid.org/0000-0002-2436-8593

Surajit Sahu and Vanessa Plantier contributed equally to this work
Françoise Watrin and Jean-Bernard Manent are Co-senior authors

Abstract

The neocortex is a 6-layered laminated structure with a precise anatomical and functional organization ensuring proper function. Laminar positioning of cortical neurons, as determined by termination of neuronal migration, is a key determinant of their ability to assemble into functional circuits. However, the exact contribution of laminar placement to dendrite morphogenesis and synapse formation remains unclear. Here we manipulated the laminar position of cortical neurons by knocking down doublecortin (Dcx), a crucial effector of migration, and show that misplaced neurons fail to properly form dendrites, spines, and functional glutamatergic and GABAergic synapses. We further show that knocking down Dcx in properly positioned neurons induces similar but milder defects, suggesting that the laminar misplacement is the primary cause of altered neuronal development. Thus, the specific laminar environment of their fated layers is crucial for the maturation of cortical neurons, and influences their functional integration into developing cortical circuits.

Key words: circuit formation, cortical lamination, dendritogenesis, neocortex, synaptogenesis

Introduction

Histogenesis of the neocortex relies on intricate developmental events eventually leading to the formation of a laminated, 6-layered structure. The laminar distribution of neocortical neurons is closely linked to their ability to assemble into appropriate circuits, thereby ensuring proper cortical function. Accordingly, altered laminar positioning resulting from neuronal migration disorders is associated with clinical symptoms such as epilepsy and intellectual disability (Guerrini and Dobyns 2014; Watrin et al. 2015; Desikan and Barkovich 2016).

Although neocortical cytoarchitecture has long been described, developmental mechanisms underlying the establishment of neuronal connectivity remain partly unknown. Once generated from progenitors, neocortical neurons undergo extensive migration before they settle into their target layers. While migrating, neurons extend 2 types of processes: a leading process at their front end, and a trailing process behind. Although the trailing process

is already defined as a growing axon (Schwartz et al. 1991; Auladell et al. 1995; Noctor et al. 2004), the leading process will become the apical dendrite only after migration has ended (Tabata and Nakajima 2001; Hatanaka and Murakami 2002). Therefore, a tight temporal and functional coupling exists between the eventual positioning of neocortical neurons defined by termination of migration, and the subsequent morphogenesis of dendrites. Pyramidal neurons of the neocortex are highly polarized cells, displaying apical and basal dendritic arbors. Synapses being formed at precise locations on dendritic spines, the size and shape of dendritic arbors are key determinants for the number and distribution of synaptic contacts. However, the exact contribution of laminar positioning to dendrite morphogenesis and synapse formation remains unclear.

In the present study, we investigated whether and how a laminar misplacement may influence the morphological and functional maturation of neocortical neurons. We induced altered laminar positioning through in utero knockdown of doublecortin (Dcx), a well-known effector of migration, and analyzed how ectopic neurons developed postnatally. We observed significant changes in dendrite and spine morphologies accompanied by altered glutamatergic and GABAergic synaptic transmission. We also evaluated the relative contributions of laminar misplacement and Dcx to these changes. Our data indicate that, besides a mild influence of Dcx on neuronal maturation, ectopic neuronal positioning is a major contributor to the altered dendritic morphogenesis and impaired development of functional glutamatergic and GABAergic synapses.

Materials and Methods

Animals

Animal experiments were performed in agreement with European directive 2010/63/UE and received approval from the French Ministry for Research, after ethical evaluation by the institutional animal care and use committee of Aix-Marseille University [protocol number: 2015040809544569_v2 (APAFIS#436)].

All experimental and control animals were generated by in utero electroporation at embryonic day 15 (E15) as described previously (Petit et al. 2014). Briefly, timed pregnant Wistar rats (Janvier) were anesthetized either with a mix of ketamine (Imalgene 1000 at 100 mg/kg) and xylazine (Rompun 2% at 10 mg/ kg) or with sevoflurane 4%. Sevoflurane anesthetized rats received buprenorphine (Buprecare at 0.03 mg/kg) 30 min before surgery. Uterine horns were exposed and a mix of plasmids (see below) and fast green was injected by pressure (PV 820 Pneumatic PicoPump; World Precision Instruments, Sarasota, FL) in the lateral ventricles of embryos through pulled glass capillaries (Drummond Scientific). Electroporations were accomplished by discharging a capacitor with a sequencing power supply (BTX ECM 830 electroporator; BTX Harvard Apparatus, Holliston, MA). The voltage pulse (40 V) was discharged across tweezer-type electrodes (Nepa Gene Co, Chiba, Japan) pinching the head of each embryo through the uterus. Resulting electroporation zones are located in the somatosensory cortex of the right hemisphere.

To induce ectopic positioning of neurons, we electroporated plasmids encoding shRNAs targeting the 3′ untranslated region (3′UTR) of Dcx (mU6pro-3′UTRhp ("Dcx-shRNA"); gift from Joe Loturco (Bai et al. 2003)). For control, we used plasmids encoding ineffective shRNAs with 3 point mutations to create mismatches (mU6pro-3′UTR-mismatch; gift from Joe Loturco (Bai et al. 2003)). Whereas the former construct efficiently knocks down Dcx expression in vivo, the latter construct is ineffective

in causing Dcx knockdown (see Fig. S1 and (Bai et al. 2003)). The co-electroporation of plasmids encoding the mCherry (pUbiquitin-mCherry; gift from I. Medyna), the red fluorescent protein RFP (pCAG-mRFP; Addgene #28311) or the enhanced green fluorescent protein eGFP (pCAG-GFP; Addgene #11150) allowed visualization of electroporated neurons. Postsynaptic sites were genetically labeled with a conditional floxed-stop plasmid expressing PSD-95-GFP (pCALSL-PSD-95-GFP; gift from Hiroshi Kawasaki (Ako et al. 2011)) or GFP-gephyrin (pCALSL-GFP-gephyrin; gift from Hiroshi Kawasaki (Ako et al. 2011)). Recombination of this plasmid was induced by the co-electroporation of a 4-hydroxy-tamoxifen (4-OHT)–activable form of Cre recombinase (pCAG-ERT2CreERT2; Addgene #13777). To generate Dcx-pKD animals, the sequences targeting the Dcx 3′ UTR from the mU6pro-3′UTRhp were cloned into the conditional floxed-stop miR-30 plasmid (pCALSL-miR30; Addgene #13786) giving rise to the pCALSL-mir30-3′UTRhp ("floxed-stop-Dcx-shmiRNA"). The use of such shmiRNAs, undergoing a more natural miRNA processing, was shown to overcome the off-target effects of shRNAs, yet producing equally efficient knockdown (see Supplemental Fig. S1 and (Baek et al. 2014)). Mismatch sequences identical to those of the control plasmid mU6pro-3′UTR-mismatch were cloned in the pCALSL-miR30 plasmid to generate the control plasmid pCALSL-mir30-3′UTR-mismatch. All plasmids were injected at a concentration of 1 μg/μL excepted the pUbiquitin-mCherry and pCAG-GFP which were injected at a concentration of 0.5 μg/μL. Cre-ERT^2-dependent recombination was carried out by injecting pups with a single intraperitoneal shot of 4-OHT (Sigma, 2 mg/mL diluted in corn oil (Sigma), 120–160 μg/ pup) at P1.

Electrophysiological Recordings

Animals were anesthetized and then decapitated. The brain was removed rapidly and transverse 300 μm thick slices were cut using a LeicaVT1200S tissue slicer in a solution containing the following (in mM): 110 choline, 2.5 KCl, 1.25 NaH$_2$PO$_4$, 25 NaHCO$_3$, 7 MgCl$_2$, 0.5 CaCl$_2$, and 7 D-glucose, 300 ± 10 mOsm, pH 7.4 (4 °C). Slices were transferred for rest (at least 1 h) at room temperature in oxygenated normal artificial cerebrospinal fluid (ACSF) containing the following (in mM): 126 NaCl, 3.5 KCl, 1.2 NaH$_2$PO$_4$, 26 NaHCO$_3$, 1.3 MgCl$_2$, 2.0 CaCl$_2$, and 10 D-glucose, 300 ± 10 mOsm, pH 7.4.

Individual slices were then transferred to the recording chamber, where they were superfused with ACSF at 30 ± 1 °C at a rate of 2–3 mL/min. Electropororated/non-electroporated cells in layer 5 were recorded in whole cell configuration in voltage-clamp mode with borosilicate glass micropipette (resistance 6–8 mΩ) containing (in mM): 130 CsGlu, 10 CsCl, 0.1 CaCl$_2$, 1.1 EGTA, 10 HEPES, 4 Mg$_2$+ATP, 0.3 Na + GTP, pH 7.22, 279 mOsm. To record miniature currents, 1 μM TTX (Tocris, UK) was added in ACSF and recordings were started after network activity had stopped (typically 5–10 min after TTX addition). Cells were clamped at –70 mV for mEPSCs 3 min-long recordings and then at 0 mV to record mIPSCs for another 3 min. Biocytin (0.5%, Sigma, USA) was added to the pipette solution for post hoc reconstruction.

Whole-cell measurements were made using a Multiclamp 700B amplifier (Axon Instruments, Molecular Devices, USA) with a Digidata 1440 A (Molecular Devices) and acquired using pCLAMP 10.3 software (Molecular Devices, USA). Signals were analyzed off line using MiniAnalysis 6.0.7 (Synaptosoft, USA) by the experimenters blind to experimental conditions.

Immunostaining

Animals were transcardially perfused with AntigenFix (Diapath) at P14–15. Their brains were then removed and postfixed in AntigenFix for 24 h before they were sectioned (100 μm) with a vibratome (Leica VT 1000 S) and processed for immunohistochemistry as free-floating sections. The mCherry signal was amplified using an anti-RFP rabbit antibody (1/1000, Rockland). Sections used for electrophysiology were fixed overnight in AntigenFix before biocytin was revealed with Alexa647-conjugated-streptavidin (1/200, Jackson ImmunoResearch). In all cases, sections were incubated with antibodies for 72 h at room temperature to increase antibody penetration into the tissue. Sections were counterstained with Hoechst (Thermo Fisher, 1/1000) and mounted in Fluoromount (Thermo Fisher).

Fluorescence Microscopy

Images used to measure angles from ectopic neurons were acquired using an Olympus BX40 fluorescence microscope with ×4 and ×10 objectives.

For 3D reconstructions, ectopic Dcx[+] and Dcx-KD neurons were imaged as 3D stack using a Zeiss LSM 510 confocal microscope with a ×20 objective and 0.5 μm z-step.

All other images were acquired as 3D stacks using a 0.3 μm z-step on a Leica TCS SP5 X confocal microscope. For the morphological analyses of ectopic/layer V and Mismatch/Dcx-pKD dendritic trees, neurons were imaged using a ×63 oil objective, roughly placing the soma at the center of the image. During the same imaging session, dendrites were imaged by using the same objective and adding a 4.5 numerical zoom. Only dendrites within 5–80 μm of the soma were imaged. When 2 channels were used, acquisitions were always sequential to avoid cross-talk. After electrophysiological recordings, a ×40 oil objective was used to image the biocytin-filled neurons.

Electron Microscopy

PSD-95-GFP electroporated P15 rats were deeply anesthetized and transcardially perfused with AntigenFix (Diapath)/0.3% glutaraldehyde (Sigma). Brains were dissected out and postfixed overnight in Antigen Fix, at 4 °C. The 120 μm coronal sections were prepared using a vibratome. PSD-95-GFP electroporated sections were selected under an epifluorescence microscope, cryoprotected in 25% sucrose in PBS overnight at 4 °C and submitted to 2 cycles of freezing on dry ice and thawing, for permeabilization. Selected sections were incubated in blocking buffer (PBS, 5% BSA, 0.1% cold water fish skin (CWFS) gelatin, 10% normal goat serum (NGS), 15 mM NaN3 pH 7.4) for 1 h at room temperature, incubated with a chicken anti-eGFP antibody (1/1000, Aves) in antibody buffer (PBS, 0.8% BSA, 0.1% CWFS gelatin, 5% NGS, 15 mM NaN3 pH 7.4) for 72 h, at 4 °C, washed and further incubated with a gold-coated IgG goat antichicken antibody (1/50, Aurion, "Ultra small 0.8 nm," Cat N° 800.244) in the same buffer for 16 h at 4 °C. Sections were washed and postfixed in PBS/2.5% glutaraldehyde at room temperature for 30 min. The sections were treated with the Aurion R-Gent silver enhancement kit (Electron Microscopy Sciences) and postfixed with 0.5% osmium tetroxide in PBS at room temperature for one hour. The sections were dehydrated in a graded series of ethanol from 30% to 70% and stained overnight in 2% uranyl acetate in 70% ethanol at 4 °C. The sections were further dehydrated in a graded series of ethanol from 70 % to 100%, washed with propylene oxide, embedded in Araldite resin. The 80 nm sections were made with an ultramicrotome (Leica, EMUC7),

analyzed with an electron microscope (Zeiss EM 912). Images were acquired with a digital camera (Bioscan 792).

Image Analysis

All neurons analyzed were located in the S1 area of the somatosensory cortex and image analyses were performed with the scientist blinded to the experimental conditions.

Orientation

To measure the orientation of apical dendrites, a radial analysis (with respect to the soma) of their angular deviation from the normal pia-directed orientation (grey area depicted in Fig. 1C, bottom panels) was performed. Polar histograms were computed with 18 bins (20° per bin), and the number of neurons per bin was plotted. Neurons for which the apical dendrite orientation lies between ±10° from the vertical axis were considered as normally oriented.

Reconstructions

Neurons were reconstructed tree-dimensionally using Neurolucida software version 10 (MBF Bioscience) from 3D stack images. The digital reconstructions were analyzed with the software L-Measure to measure the number of primary branches and the total number of ramifications of each neuron (Scorcioni et al. 2008). Comparisons between groups were done directly in L-Measure.

Synaptogenesis

PSD-95-GFP[+] puncta were manually counted on the 3D stack using the Cell counter plugin of FIJI (Schindelin et al. 2012) and the length of the corresponding dendrite was measured in the same software. The linear density of PSD-95-GFP[+] puncta was calculated as the ratio of these 2 measurements.

Dendritic spine density and morphology were analyzed from 2D images generated by maximum intensity projection of the 3D stacks in FIJI and converted to RGB images. The length, head width and neck width of dendritic spines were then manually traced on SynPAnal (Danielson and Lee 2014). Only spines clearly protruding from the dendritic shaft were reconstructed. A 700 nm wide circle was then generated around each spine head and PSD-95-GFP[+] puncta were detected using a fluorescence threshold to count the proportion of spines containing puncta. This detection was manually edited to remove false positive. The same thresholded images were used to establish the percentages of puncta on dendritic shafts and spines in SynPAnal.

GFP-gephyrin[+] puncta were analyzed from maximum intensity projection of 3D stack in FIJI. Puncta were semi-automatically detected using the "Analyse particles" tool in FIJI after thresholding of the images. The linear density of GFP-gephyrin[+] puncta was calculated as the number of puncta divided by the length of the corresponding dendrites.

Synaptosome Preparation and Western Blot Analysis

Cortices from P10, P15, and P20 rats were homogenized in Syn-PER™ synaptic protein extraction reagent (ThermoScientific) complemented with protease and phosphatase inhibitors (Pierce, ThermoScientific) in a Dounce homogenizer (1 mL/100 mg of tissue) at 4 °C. The homogenates were centrifuged at $1000 \times g$ for 10 min at 4 °C and the supernatants further centrifuged at $15\,000 \times g$ for 20 min at 4 °C. The supernatants (cytosolic fractions) were collected and the pellets (synaptosome fractions) were
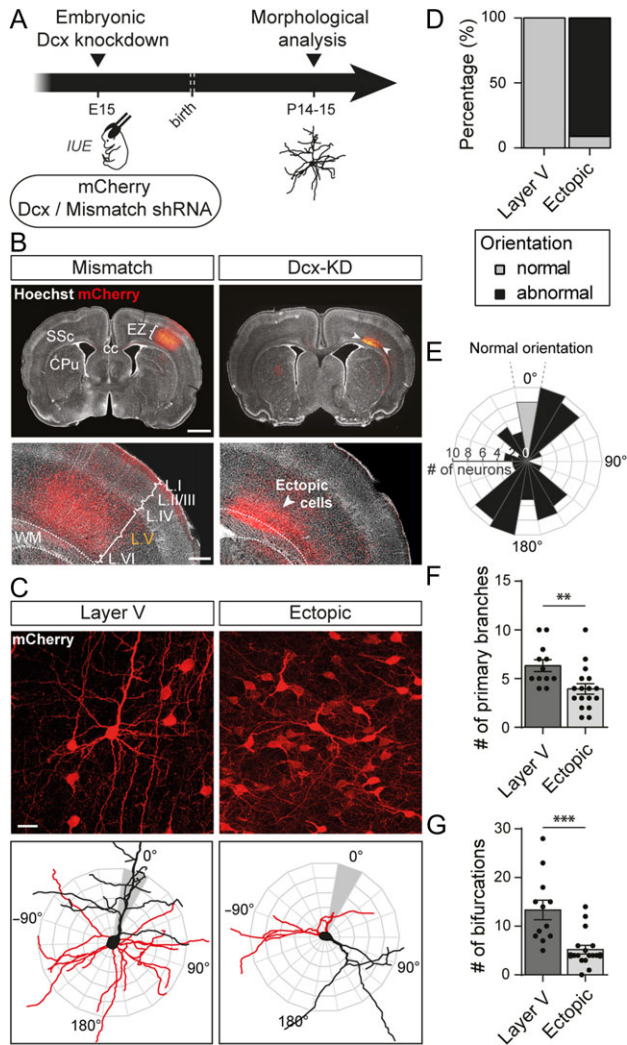
Figure 1. Altered neuronal positioning impairs neuronal polarity and morphology. (A) Schematic of the experimental timeline. Embryos were electroporated in utero at E15 with a plasmid encoding a short hairpin RNA (shRNA) targeting Dcx 3′UTR to create an embryonic Dcx knockdown or with a mismatch shRNA for control. A second plasmid encoding a red fluorescent protein, mCherry, was co-electroporated to spot the electroporated neurons. IUE: in utero electroporation (B) Representative neocortical sections showing that mismatch neurons are properly placed in layer (L) V of the somatosensory cortex (SSc) while Dcx-KD neurons are located ectopically between the corpus callosum (cc) and layer VI of the cortex at P14. Dotted lines delineate the white matter (WM). EZ = electroporation zone; CPu = caudate putamen. Top panels, scale bar = 2 mm. Bottom panels, scale bar = 500 μm. (C) High magnification confocal images of layer V and ectopic neurons used to reconstruct their dendritic arbors (top panels). The 3D reconstructions are superimposed on orientation diagrams used to score apical dendrite orientation in (E) (bottom panels). Red: basal arbor; black: apical arbor and soma. Scale bar = 100 μm. (D) Stacked bar graph showing the percentage of normally or abnormally oriented neurons in each set of data analyzed in (F) and (G). (E) Polar histogram of apical dendrite orientation (in degrees) in ectopic neurons. Bars represent the number of neurons with a similar apical dendrite orientation in 20° bins. Properly oriented neurons are plotted in grey. Neuronal somata are located at the center as depicted in (C). (F,G) Quantification of the mean number of primary branches (F) and bifurcations (G) in 3D reconstructions from layer V and ectopic neurons. Values are given as mean ± SEM. Each dot represents a neuron. (F) t-test, P-value < 0.0074; (G) Mann–Whitney test, P-value < 0.0001.

resuspended in 200 μL of Syn-PER reagent, with protease and phosphatase inhibitors (Pierce, ThermoScientific). Proteins from cytosolic fractions and synaptosomes samples were quantified

using a bicinchronic acid (BCA) Protein Assay Kit (Pierce, ThermoScientific). 20 μg of proteins were loaded per well, subjected to 7.5% sodium-dodecyl sulfate-polyacrylamide gel electrophoresis (SDS-PAGE) (Criterion™ TGX™ precast gels, Bio-Rad Laboratories) and transferred to Immun-blot LF PVDF membranes (Bio-Rad Laboratories). Membranes were blocked for 1 h and incubated overnight with rabbit polyclonal anti-Dcx (1/1000, Abcam, Cat No AB18723) and rabbit monoclonal anti-PSD-95 (D74D3) (1/1000, Cell Signaling, Cat No 3409S) antibodies. Membranes were then incubated with an Alexa Fluor 647 goat anti-rabbit antibody (1/500, Invitrogen) for 1 h. Image acquisitions were performed with a CDD camera (GBox, Syngene). The membranes were incubated in stripping buffer (62.5 mM Tris–HCl pH 6.8, 2% SDS, 100 mM β-mercaptoethanol) at 55 °C for 30 min, blocked and reincubated with a mouse anti-α-tubulin (DM1A) antibody (1/5000, ThermoScientific, Cat No 62204) for 4 h. Membranes were washed and incubated with an Alexa Fluor 488 goat anti-mouse antibody (1/500, Invitrogen, Cat No A11001) for 1 h and imaged.

Statistics

All statistical analyses were performed using Prism 6 (Graphpad). Normality of the data distributions was systematically tested using d'Agostino & Pearson test and Shapiro–Wilk test. Comparison of groups was subsequently tested with unpaired t-tests for normal data sets or Mann–Whitney tests for non-normal data sets. Two-sample Kolmogorov–Smirnov tests were used to compare distributions of data obtained from electrophysiological experiments. All tests were 2-tailed and the level of significance was set at $P < 0.05$. Statistical power was checked in all experiments to ensure sample sizes were adequate. n refers to the number of cells, except for spine morphology analyses where it refers to the number of spines; N refers to the number of animals.

Results

Ectopic Neurons Fail to Develop Proper Dendritic Arbors and Spines

To study whether a correct laminar positioning may influence the morphological and functional maturation of neocortical neurons, we disturbed neuronal migration by knocking down Dcx in utero. At Embryonic day 15 (E15), a plasmid encoding a short hairpin RNA (shRNA) targeting Dcx (Dcx-shRNA) was electroporated in the cortical progenitors of rat embryos (Bai et al. 2003) (Fig. 1A). Co-electroporation of a plasmid encoding the red fluorescent protein mCherry allowed visualization of the electroporated neurons in postnatal stages. At Postnatal days 14–15 (P14–15), mCherry⁺ neurons electroporated with Dcx shRNA had failed to migrate and were located ectopically within the white matter, as previously described. By contrast, in control brains electroporated with a Dcx-mismatch shRNA, mCherry⁺ neurons migrated properly into layer V (Fig. 1B).

To analyze whether altered neuronal positioning has an impact on neuronal polarity and overall morphology, we imaged ectopic neurons from Dcx knockdown (Dcx-KD) brains compared with layer V neurons from mismatch brains and scored their apical dendrite orientation (Fig. 1C–E). Apical dendrites of layer V neurons were 100% (12/12 neurons from 6 animals) radially oriented towards the cortical surface whereas less than 10% (79/87 neurons from 5 animals) of ectopic pyramidal neurons were oriented properly. The remaining ectopic neurons were either oriented aberrantly or presented an abnormal bipolar morphology, preventing us from clearly defining an

apical dendrite. We then checked whether altered cortical positioning influenced dendritic growth by reconstructing the dendritic arbor and analyzing the complexity of basal dendrites. Ectopic neurons grew significantly fewer primary branches than layer V neurons (6.3 ± 0.6 vs. 3.9 ± 0.5; t-test, P = 0.0074; n = 12 layer V neurons, 17 ectopic neurons; N = 6 animals/condition) and their dendritic arbor was less ramified (13.3 ± 2 vs. 5.2 ± 0.9; Mann–Whitney test, P < 0.0001; n = 12 layer V neurons, 17 ectopic neurons; N = 6 animals/condition) (Fig. 1F,G).

To evaluate the impact of altered positioning and dendritic growth on spine formation, we manually reconstructed the spines from the mCherry signal amplified by immunohistochemistry (Fig. 2A). In ectopic neurons, the linear density of spines was decreased by 40% compared with control neurons in layer V (35.6 ± 3.2 vs. 21.6 ± 2.6 spines/100 μm; t-test, P = 0.0024; n = 13 neurons/condition; N = 6 animals/condition) (Fig. 2B). In addition, successfully formed spines had an altered morphology including wider heads (0.498 ± 0.005 vs. 0.535 ± 0.01 μm; Mann–Whitney test, P < 0.0001; n = 1953 spines from 13 layer V neurons and 501 spines from 13 ectopic neurons; N = 6 animals/condition) and wider necks (0.27 ± 0.002 vs. 0.39 ± 0.009 μm; Mann–Whitney test, P < 0.0001; n = 1953 spines from 13 layer V neurons and 501 spines from 13 ectopic neurons; N = 6 animals/condition) although their length was comparable to spines from layer V neurons (1.281 ± 0.015 vs. 1.281 ± 0.034 μm; Mann–Whitney test, P = 0.15; n = 1953 spines from 13 layer V neurons and 501 spines from 13 ectopic neurons; N = 6 animals/condition) (Fig. 2C–E). Together, these data suggest that an appropriate positioning ensures proper cell polarity, dendritic growth and spine morphology.
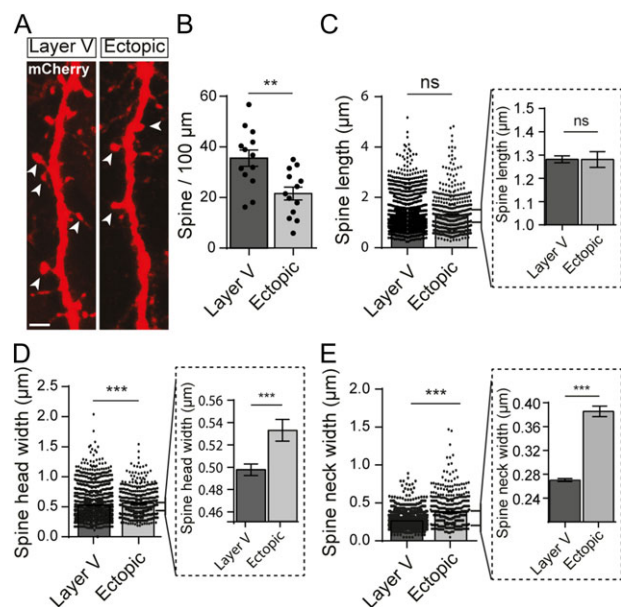

Figure 2. Ectopic neurons display a reduced spine density and altered spine morphology. (A) High magnification confocal images of dendrites from layer V and ectopic neurons electroporated with mCherry. Representative dendritic spines are indicated by arrow heads. Scale bar = 2 μm. (B) Bar graph illustrating the mean number of spines per 100 μm of dendrite. Values are given as mean ± SEM. Each dot represents a neuron. t-test, P-value = 0.0024. (C–E) Quantification of the mean dendritic spine length (C), head width (D), and neck width (E) in layer V and ectopic neurons. Values are given as mean ± SEM. Each dot represents a spine. Bar graphs in dotted line frames are higher magnifications of the initial bar graphs. (D,E) Mann–Whitney test, P-value < 0.0001.

Glutamatergic Synaptogenesis is Altered in Ectopic Neurons

Because dendritic spines are the sites of most excitatory synapses, the spine alterations reported above could be associated with impaired glutamatergic synaptogenesis. To check this point, glutamatergic postsynapses were genetically labeled with PSD-95-GFP, a scaffolding protein that anchors glutamate receptors and had been fused with GFP. We co-electroporated a floxed-stop-PSD-95-GFP plasmid at E15 with plasmids encoding Dcx shRNA, mCherry and a tamoxifen-inducible Cre-recombinase. The Cre-recombinase was activated at P1 by intraperitoneal injection of tamoxifen to induce PSD-95-GFP expression (Fig. 3A). A single tamoxifen injection induced a low level of recombination and allowed for a sparse labeling of PSD-95-GFP, making it easier to follow dendrites of individual neurons (Fig. 3B). Once expressed, PSD-95-GFP proteins formed puncta localized mainly on spine heads, where the postsynapse is usually assembled in mature neurons (Fig. 3C). Electron microscopy experiments confirmed that PSD-95-GFP was localized in spines near the electron dense postsynaptic density (PSD) facing presynaptic elements containing vesicles (Fig. 3D). We then quantified the linear density of PSD-95-GFP+ puncta along dendritic segments localized within 5–80 μm of the soma. In ectopic neurons, the mean density of PSD-95-GFP+ puncta was significantly lower than in layer V neurons (87.54 ± 4.03 vs. 15.31 ± 2.53 puncta/100 μm; t-test, P < 0.0001; n = 13 neurons/condition; N = 6 animals/condition) (Fig. 3E,F), suggesting that ectopic neurons form less glutamatergic synapses. In layer V neurons, 54% (554/1020) of these puncta were located on dendritic spines (n = 6 neurons from 4 animals) (Fig. 3G). On the contrary, in ectopic neurons, only 20% of PSD-95-GFP+ puncta were located on spines and 80% (129/161) were found on the dendritic shaft (n = 6 neurons from 4 animals), suggesting that ectopic neurons might be less mature than their properly placed counterparts. In addition, because spines containing PSD-95 are generally classified as more differentiated (Berry and Nedivi 2017), we analyzed the proportion of those containing PSD-95-GFP+ puncta in ectopic and layer V neurons. In ectopic neurons, about 90% (180/217) of spines analyzed were devoid of PSD-95-GFP+ puncta (n = 6 neurons from 4 animals) whereas this fraction was only of 24% (199/621) in layer V neurons (n = 6 neurons from 4 animals) (Fig. 3F,H). Thus, in addition to a decreased spine density, ectopic neurons form less spines with a mature PSD scaffold.

To investigate whether a reduced density of spines and a reduced PSD scaffold translate into altered synaptic transmission, we recorded miniature excitatory currents (mEPSC) from electroporated neurons (Fig. 4A,B). We successfully recorded mEPSCs in ectopic neurons, indicating that these cells received synaptic inputs. However, cumulative frequency curves of mEPSC inter-event intervals revealed a significant shift towards higher values, suggesting a decreased frequency of mEPSCs in ectopic neurons as compared with layer V neurons (Kolmogorov–Smirnov test, P < 0.0001; n = 8114 events from 15 layer V neurons, 5364 events from 18 ectopic neurons; N = 3–4 animals) (Fig. 4C). This decreased frequency of mEPSCs is in accordance with our previous results suggesting that ectopic neurons form less synapses. Additionally, we analyzed the amplitude and half-width of events occurring in ectopic neurons and compared them to those of layer V neurons. The cumulative frequency curve of mEPSC amplitude was shifted towards higher values in ectopic neurons, indicating an increased amplitude of mEPSCs in this population (Kolmogorov–Smirnov test, P < 0.0001; n = 1348 events from 14 layer V neurons, 1221 events from 18 ectopic neurons; N = 4–5 animals) (Fig. 4D). The
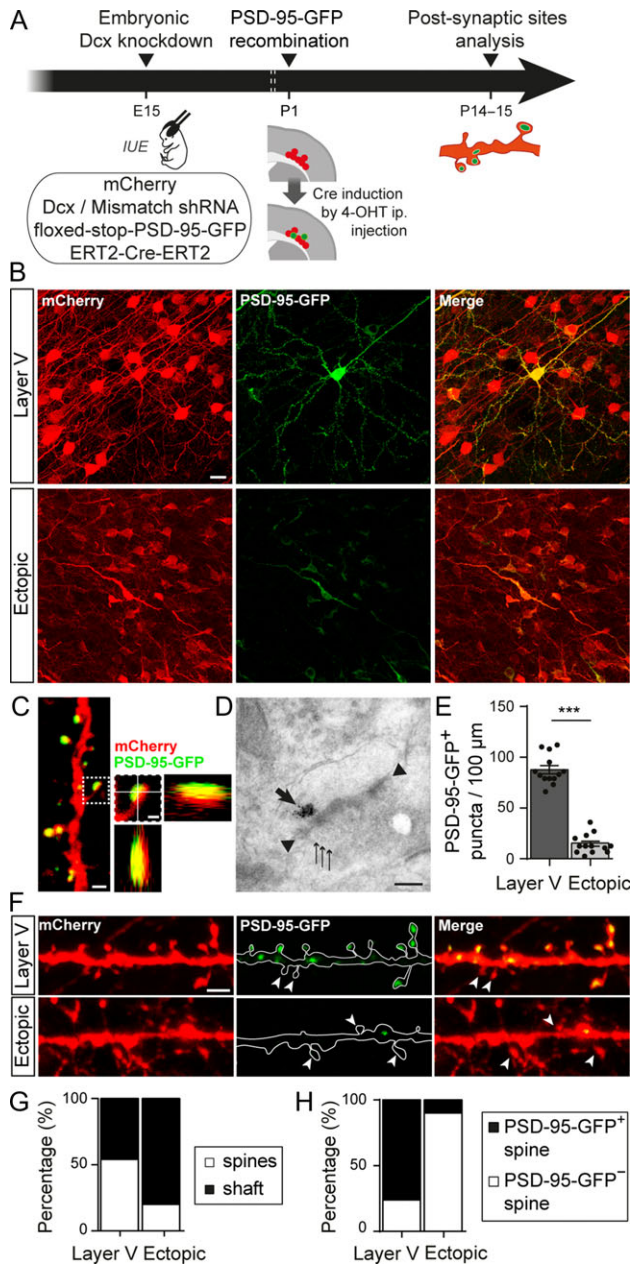
Figure 3. Altered neuronal positioning decreases the density of glutamatergic synapses. (A) Animals were electroporated at E15 with 3 plasmids encoding for the fluorescent marker mCherry, a Dcx or mismatch shRNA and a tamoxifen activable Cre-recombinase (ERT^2-Cre-ERT^2). A fourth conditional plasmid was co-electroporated to express the postsynaptic glutamatergic protein PSD-95-GFP (floxed-stop-PSD-95-GFP). Sparse recombination of the floxed-stop-PSD-95-GFP plasmid was induced in a subset of electroporated neurons through a single intraperitoneal (i.p.) injection of 4-hydroxytamoxifen (4-OHT) at P1. Glutamatergic postsynaptic sites were analyzed at P14–15. IUE: in utero electroporation. (B) Confocal images of the electroporated zone (red) showing sparse recombination of the floxed-stop-PSD-95-GFP plasmid (green) following 4-OHT injection. Scale bar = 20 μm. (C) High magnification confocal image of a dendrite with PSD-95-GFP$^+$ spines. On the right, higher magnification of one dendritic spine and its orthogonal views show that the PSD-95-GFP$^+$ punctum colocalizes with the mCherry filled spine. Left image scale bar = 1 μm; right image scale bar = 0.5 μm. (D) Electron microscopy image of a PSD-95-GFP$^+$ postsynapse facing a presynaptic compartment containing vesicles. The thick arrow shows immunogold labeled PSD-95-GFP proteins; arrow heads show electron-dense thickening of the postsynaptic membrane; thin arrows show presynaptic vesicles. Scale bar = 0.2 μm. (E) Bar graphs and scatter dot plots illustrating the density of PSD-95-GFP$^+$ puncta per 100 μm of dendrites in layer V and ectopic neurons. Values are given as

half-width curve showed a minor, although significant, shift towards smaller values (Kolmogorov–Smirnov test, $P < 0.0001$; $n = 1348$ events from 14 layer V neurons, 1221 events from 18 ectopic neurons; $N = 4$–5 animals) (Fig. 4E). Overall, our data suggest that migration into the appropriate layer is important for dendritic growth, spine formation and glutamatergic synaptogenesis, both on a morphological and functional level.

Dcx Impacts Spine Morphology and Glutamatergic Synaptogenesis

The experimental paradigm we used relies on Dcx knockdown to induce ectopic positioning of neurons. Therefore, we cannot rule out that the developmental defects we observed were directly due to Dcx knockdown, independently of the position of neurons. For this reason, it was important to check if Dcx plays a role in dendritic growth, spine formation or glutamatergic synaptogenesis.

Bai et al. previously reported (Bai et al. 2003) that non-electroporated neurons are present amongst the ectopic cells aggregated within the white matter (Fig. 5A,B). Although these cells are ectopic, they expressed Dcx during their development ("ectopic Dcx$^+$ neurons") unlike electroporated neurons ("ectopic Dcx-KD neurons"). We recorded mEPSCs from both populations to check if the development and function of glutamatergic synapses were affected by Dcx-KD (Fig. 5B,C). The inter-event interval distribution was shifted towards lower values in ectopic Dcx$^+$ neurons indicating a higher frequency of mEPSCs in neurons that expressed Dcx during development (Kolmogorov–Smirnov test, $P < 0.0001$; $n = 4771$ events from 10 ectopic Dcx$^+$ neurons, 5364 events from 18 ectopic Dcx-KD neurons; $N = 3$–4 animals) (Fig. 5D). Moreover, the cumulative frequency curve of mEPSC amplitude was slightly, but significantly, changed (Kolmogorov–Smirnov test, $P = 0.0067$; $n = 1049$ events from 10 ectopic Dcx$^+$ neurons, 1221 events from 18 ectopic Dcx-KD neurons; $N = 3$–4 animals) and the cumulative frequency curve of mEPSC half-width was shifted towards higher values in ectopic Dcx$^+$ neurons (Kolmogorov–Smirnov test, $P < 0.0001$; $n = 1049$ events from 10 ectopic Dcx$^+$ neurons, 1221 events from 18 ectopic Dcx-KD neurons; $N = 3$–4 animals) (Fig. 5E,F). Following the electrophysiological recordings, neurons were filled with biocytin and reconstructed to analyze their overall morphology (Fig. 5B,G). As reported above, most ectopic Dcx-KD neurons were aberrantly oriented or presented an abnormal morphology preventing us to define an apical dendrite (10/11 neurons from 4 animals). In most cases, ectopic Dcx$^+$ neurons were able to form an apical dendrite but were not oriented properly towards the cortical surface (6/7 neurons from 3 animals) (Fig. 5H). Analysis of the basal dendritic arbor revealed no significant difference in the number of primary branches formed by ectopic Dcx$^+$ and Dcx-KD neurons (4.29 ± 0.78 vs. 2.73 ± 1.42; Mann–Whitney test, $P = 0,145$; $n = 7$ ectopic Dcx$^+$ neurons, 11 ectopic Dcx-KD neurons; $N = 3$–4 animals) (Fig. 5I). However, ectopic Dcx$^+$ neurons were more ramified than ectopic Dcx-KD neurons, indicating that Dcx might play a role in the formation of the dendritic arbor (10 ± 2.28 vs. 4.09 ± 0.73; Mann–Whitney test, $P = $

mean ± SEM. t-test, P-value < 0.0001. (F) Confocal images of mCherry$^+$ dendrites and PSD-95-GFP$^+$ puncta from layer V and ectopic neurons. Arrow heads indicate spines devoid of PSD-95-GFP$^+$ puncta. Scale bar = 2 μm. (G) Stacked bar graphs showing the relative percentages of PSD-95-GFP$^+$ puncta on dendritic spines and shafts in layer V and ectopic neurons. (H) Stacked bar graphs showing the relative percentages of PSD-95-GFP$^+$ and PSD-95-GFP$^-$ spines in layer V and ectopic neurons.
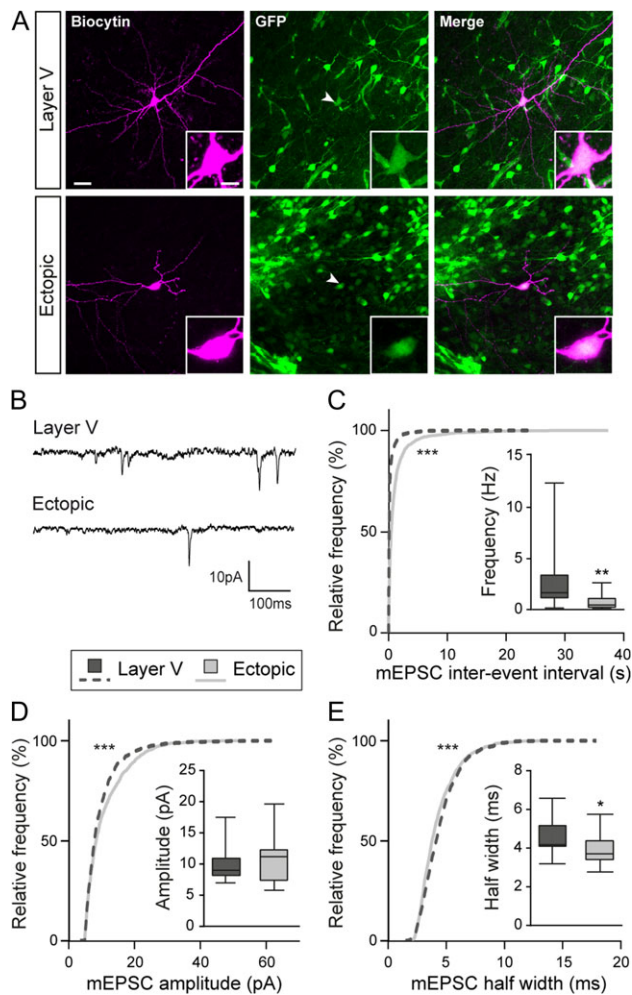
Figure 4. Miniature glutamatergic currents are impaired in ectopic neurons. (A) Confocal images of layer V and ectopic neurons filled with biocytin during electrophysiological recordings. Recorded cells were electroporated neurons as indicated by their GFP$^+$ fluorescence (arrow heads). Inserts show higher magnification images of the somas. Scale bars = 30 μm/10 μm. (B) Representative traces of the miniature excitatory postsynaptic currents (mEPSCs) recorded from layer V and ectopic neurons and analyzed in (C–E). (C–E) Cumulative distributions and box plots of the inter-event interval (C), amplitude (D), and half width (E) values of mEPSCs from layer V and ectopic neurons. Box limits indicate the 25th and 75th percentiles; whiskers extend to minimum and maximum values; horizontal lines show the medians. Kolmogorov–Smirnov test, P-value < 0.0001; Mann–Whitney test, (C) P-value = 0.0026, (D) P-value = 0.5053, (E) P-value = 0.0362.

0,027; n = 7 ectopic Dcx$^+$ neurons, 11 ectopic Dcx-KD neurons; N = 3–4 animals) (Fig. 5J). These electrophysiological and morphological differences between ectopic Dcx$^+$ and Dcx-KD neurons suggest that Dcx is involved in dendritic growth and synaptogenesis in addition to its canonic role in migration.

To further test this hypothesis, we designed a conditional knockdown strategy to silence Dcx expression after migration has ended. We electroporated at E15 a tamoxifen and Cre-dependent plasmid encoding a Dcx shRNA (floxed-stop-Dcx-shmiRNA) and induced its expression with a tamoxifen injection at P1 (Fig. 6A). This postnatal knockdown (pKD) took effect after migration had ended so Dcx-pKD neurons migrated to layer V similarly to control neurons electroporated with a mismatch shRNA (Fig. 6B). On the other hand, Dcx-pKD was induced early enough to study its effect on dendrite formation and early synaptogenesis, both events mostly occurring during the first postnatal weeks.

We first analyzed Dcx-pKD effect on neuronal polarity and morphology. We observed that 100% (9/9 neurons from 3 animals) of Dcx-pKD neurons presented a pyramid shaped soma and their apical dendrites were radially oriented towards the cortical surface, similarly to mismatch neurons (12/12 neurons from 6 animals) (Fig. 6C,D). 3D reconstructions of basal dendritic arbor revealed that they extended the same number of primary branches as mismatch neurons (5.3 ± 0.22 vs. 5.2 ± 0.49; t-test, P = 0.826; n = 12 mismatch neurons, 9 Dcx-pKD neurons; N = 3–6 animals) but these branches were less ramified (13 ± 1.42 vs. 8 ± 1.44; t-test P = 0.026; n = 12 mismatch neurons, 9 Dcx-pKD neurons; N = 3–6 animals) (Fig. 6C,E,F). These data suggest that Dcx influences dendritic growth in properly positioned neurons, although to a lesser extent than in ectopic positions.

We then checked for a potential effect of Dcx-pKD on spine density and morphology. In Dcx-pKD neurons properly placed in layer V, spine density was similar to the one in mismatch neurons (66.8 ± 5.9 vs. 56.2 ± 8.0 spines/100 μm; t-test, P = 0.296; n = 15 neurons/condition; N = 7 animals/condition) (Fig. 7A,B). Closer analysis showed that spines from both groups also had the same length (1.308 ± 0.012 vs. 1.306 ± 0.014 μm; Mann–Whitney test, P = 0.717; n = 3235 spines from 15 mismatch neurons, 2124 spines from 15 Dcx-pKD neurons; N = 7 animals/condition). However, spines had a slightly wider head (0.468 ± 0.004 vs. 0.485 ± 0.004 μm; Mann–Whitney test, P < 0.001; n = 3235 spines from 15 mismatch neurons, 2124 spines from 15 Dcx-pKD neurons; N = 7 animals/condition) and a slightly wider neck (0.264 ± 0.002 vs. 0.284 ± 0.002 μm; Mann–Whitney test, P < 0.001; n = 3235 spines from 15 mismatch neurons, 2124 spines from 15 Dcx-pKD neurons; N = 7 animals/condition) in Dcx-pKD neurons (Fig. 7C–E), suggesting a role for Dcx in spine formation.

In order to play such a role, Dcx should be present in the synaptic compartment during the first postnatal weeks. In cortical layer V neurons, very little dendritic spines are visible during this period making difficult any immunohistochemical evaluation. Therefore, we decided to analyze by Western blot cytosolic and synaptosomal fractions isolated from P10, P15, and P20 rat neocortex (Fig. 7F) and found that Dcx was enriched in the synaptosomal as compared with the cytosolic fraction. Dcx expression was also down regulated from P10 to P20, as opposed to the PSD-95 which expression increased during the same developmental period. These results agree with previous reports investigating the maturation of mouse synaptosomal proteome (Moczulska et al. 2014; Gonzalez-Lozano et al. 2016).

Because Dcx seems involved in spine formation, glutamatergic synaptogenesis could also be affected by Dcx postnatal knockdown. We quantified the density of PSD-95-GFP$^+$ puncta as described above and found that the linear density of PSD-95-GFP$^+$ puncta was similar in both groups (101.4 ± 8.8 vs. 89.1 ± 7.4 puncta/100 μm; t-test, P = 0.296; n = 16 mismatch neurons, 15 Dcx-pKD neurons; N = 7 animals/condition) (Fig. 8A,B). In mismatch neurons, 46% (2060/4432) of these puncta were found on dendritic shafts versus 56% (1776/3176) in Dcx-pKD neurons (n = 14–15 neurons/condition; N = 7 animals/condition) (Fig. 8C). Moreover, 18% (564/3123) of spines from mismatch neurons (n = 14 neurons from 7 animals) and 24% (490/2046) of spines from Dcx-pKD neurons (n = 15 neurons from 7 animals) did not contain PSD-95-GFP$^+$ puncta (Fig. 8D). Overall, our data show that the amount of PSD scaffold is mostly unaffected in Dcx-pKD neurons.

Nevertheless, the spine alterations reported above could be associated with altered synaptic transmission. We checked this point by recording mEPSCs from Dcx-pKD neurons and
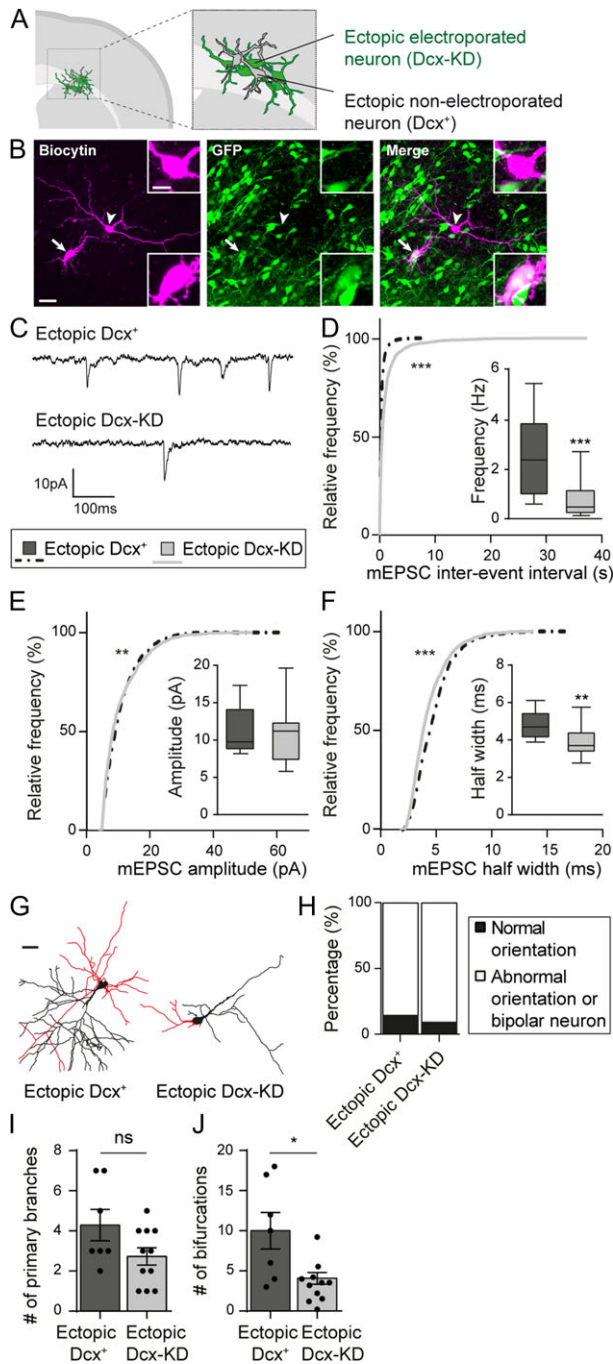
Figure 5. Dcx expression is important for glutamatergic synaptogenesis and dendritic growth. (A) Schematic depicting the presence of non-electroporated ectopic neurons amongst electroporated ectopic neurons. (B) Confocal images of ectopic neurons filled with biocytin during electrophysiological recordings. The arrow indicates an electroporated GFP+ neuron (Dcx-KD) while the arrow head shows a non-electroporated GFP- neuron (Dcx+). Side bar images show higher magnification images of the somas. Scale bars = 30 μm/10 μm. (C) Representative traces of mEPSCs recorded from ectopic Dcx+ and Dcx-KD neurons and analyzed in (D–F). (D–F) Cumulative distributions and box plots of the inter-event interval (D), amplitude (E), and half width (F) values of mEPSCs from ectopic Dcx+ and Dcx-KD neurons. Box limits indicate the 25th and 75th percentiles; whiskers extend to minimum and maximum values; horizontal lines show the medians. Kolmogorov–Smirnov test, (D,F) P-value < 0.0001, (E) P-value = 0.0067; Mann–Whitney test, (D) P-value = 0.0008, (E) P-value = 0.7868, (F) P-value = 0.006. (G) 3D reconstructions of ectopic Dcx+ and Dcx-KD neurons used to analyze their basal dendritic arbor (red) in (I) and (J). Scale bar = 30 μm. (H) Stacked bar graph showing the relative percentages of normally oriented

mismatch neurons (Fig. 8E–I). In Dcx-pKD neurons, the cumulative frequency curve of mEPSC inter-event interval was shifted towards higher values, revealing a decreased frequency of mEPSCs in Dcx-pKD neurons compared with mismatch neurons (Kolmogorov–Smirnov test, $P < 0.0001$; $n = 8438$ events from 13 mismatch neurons, 5756 events from 18 Dcx-pKD neurons; $N = 3$–5 animals) (Fig. 8G). In addition, although the cumulative frequency curve of mEPSC amplitude revealed no change in Dcx-pKD neurons compared with mismatch neurons, (Kolmogorov–Smirnov test, $P = 0.471$; $n = 1205$ events from 13 mismatch neurons, 1118 events from 13 Dcx-pKD neurons; $N = 3$–5 animals), the cumulative frequency curve of mEPSC half-width was slightly but significantly shifted towards lower values in Dcx-pKD neurons (Kolmogorov–Smirnov test, $P < 0.0001$; $n = 1205$ events from 13 mismatch neurons, 1118 events from 13 Dcx-pKD neurons; $N = 3$–5 animals) (Fig. 8H,I). Altogether, these data are consistent with the notion that Dcx, in addition to its known role on migration, influences spine formation, as well as the proper development of functional glutamatergic synapses.

Laminar Positioning and Dcx Impact GABAergic Synaptogenesis

To study whether a correct laminar positioning may also influence the development of GABA synapses, we genetically labeled GABAergic postsynapses with GFP-gephyrin, a scaffolding protein that anchors GABA$_A$ receptors and had been fused with GFP. Similarly to what was described above for PSD-95-GFP, we utilized a floxed-stop-GFP-gephyrin construct and a tamoxifen-inducible Cre to induce a sparse GFP-gephyrin expression. Once expressed, GFP-gephyrin proteins formed puncta distributed along the dendritic shaft, where most inhibitory postsynapses are usually formed (Fig. 9A). In ectopic neurons, the mean linear density of GFP-gephyrin+ puncta was significantly lower than in layer V neurons (42.69 ± 6.23 vs. 11.08 ± 2.337 puncta/100 μm; Mann–Whitney test, $P = 0.0043$; $n = 6$ neurons/condition; $N = 2$–3 animals) (Fig. 9B), suggesting that ectopic neurons form less GABA synapses. To investigate whether this reduced density of GFP-gephyrin+ puncta translates into altered GABAergic synaptic transmission, we recorded miniature inhibitory currents (mIPSC) from electroporated neurons (Fig. 9C). We detected rare mIPSCs from ectopic neurons, indicating that they received GABAergic inputs, although at a very low rate. Accordingly, cumulative frequency curves of mIPSC inter-event intervals revealed a very significant shift towards higher values, suggesting a strongly decreased frequency of mIPSCs in ectopic neurons as compared with layer V neurons (Kolmogorov–Smirnov test, $P < 0.0001$; $n = 4122$ events from 17 layer V neurons, 442 events from 17 ectopic neurons; $N = 3$–4 animals) (Fig. 9D). This was accompanied by a decreased amplitude and higher half-width of mIPSCs in ectopic neurons, as indicated by leftward and rightward shifts of cumulative frequency curves respectively (Kolmogorov–Smirnov test, $P < 0.0001$ for both amplitude and half-width; $n = 1049$ events from 17 layer V neurons, 239 events from 10 ectopic neurons; $N = 3$–4 animals) (Fig 9E, F). Together, these morphological and electrophysiological data suggest that migration into appropriate layers is crucial for GABAergic synaptogenesis.
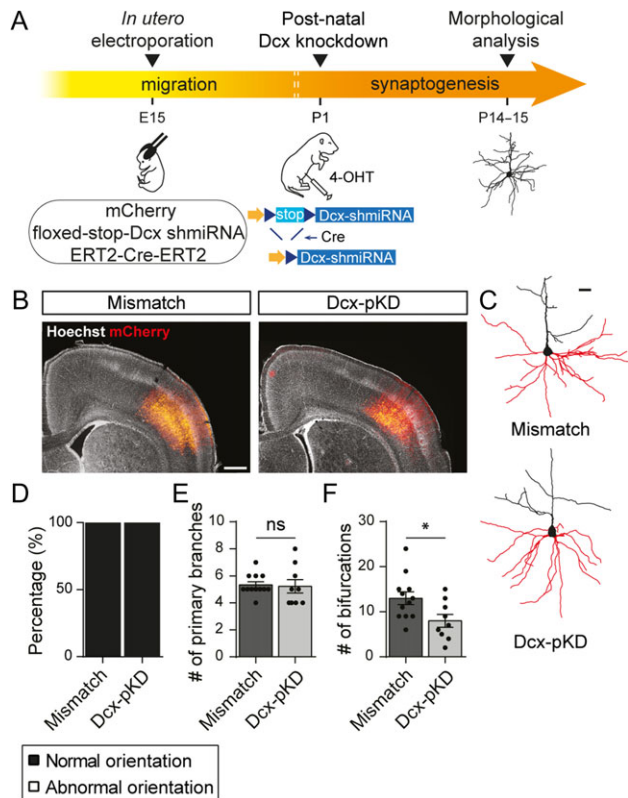
neurons and abnormally oriented or bipolar neurons analyzed in (I) and (J). (I,J) Bar graphs and scatter dot plots showing the mean number of primary branches (I) and bifurcations (J) in ectopic Dcx+ and Dcx-KD neurons. Values are given as mean ± SEM. Each dot represents a neuron. (J) Mann–Whitney test, P-value = 0.027.

Figure 6. Postnatal knockdown of Dcx induces a simplification of the dendritic arbor. (A) Schematic of the experimental timeline. Rats were electroporated at E15 with a conditional plasmid encoding for a Dcx shRNA (floxed-stop-Dcx-shmiRNA) and 2 constitutive plasmids encoding mCherry and a tamoxifen-activable Cre (ERT²-Cre-ERT²). The postnatal Dcx knockdown was induced at P1 through Cre-mediated recombination following 4-OHT intraperitoneal injection. Neurons were reconstructed at P14–15 to analyze the morphology of their basal dendritic arbor. (B) Low magnification images of electroporated cortices where electroporated neurons (red) have migrated properly to layer V both in mismatch and Dcx-pKD brains. Scale bar = 1 mm (C) 3D reconstructions of mismatch and Dcx-pKD neurons used to analyze their basal dendritic arbor (red) in (E) and (F). Scale bar = 100 μm (D) Stacked bar graph showing the relative percentages of normally oriented neurons and abnormally oriented or bipolar neurons analyzed in (E) and (F). (E,F) Bar graphs and scatter dot plots showing the mean number of primary branches (E) and bifurcations (F) in mismatch and Dcx-pKD neurons. Values are given as mean ± SEM. Each dot represents a neuron. (F) t-test, P-value = 0.026.

To test the influence of Dcx on GABAergic synaptogenesis, we first compared mIPSCs in ectopic Dcx⁺ neurons and ectopic Dcx-KD neurons, as we did earlier for mEPSCs. Cumulative frequency curves of mIPSC inter-event intervals revealed a very significant shift towards higher values, suggesting a strongly decreased frequency of mIPSCs in ectopic Dcx-KD neurons as compared with ectopic Dcx⁺ neurons (Kolmogorov–Smirnov test, P < 0.0001; n = 2937 events from 12 ectopic Dcx⁺ neurons, 442 events from 17 ectopic Dcx-KD neurons; N = 2–3 animals) (Fig. 9G). This was accompanied by a decreased amplitude and higher half-width of mIPSCs in ectopic Dcx-KD neurons, as indicated by a leftward and rightward shift of cumulative frequency curves, respectively (Kolmogorov–Smirnov test, P < 0.0001 for both amplitude and half-width; n = 960 events from 12 ectopic Dcx⁺ neurons, 239 events from 10 ectopic Dcx-KD neurons; N = 2–3 animals) (Fig. 9H–I). Together, these electrophysiological differences between ectopic Dcx⁺ and Dcx-KD neurons suggest that Dcx has an influence on GABA synapses formation.
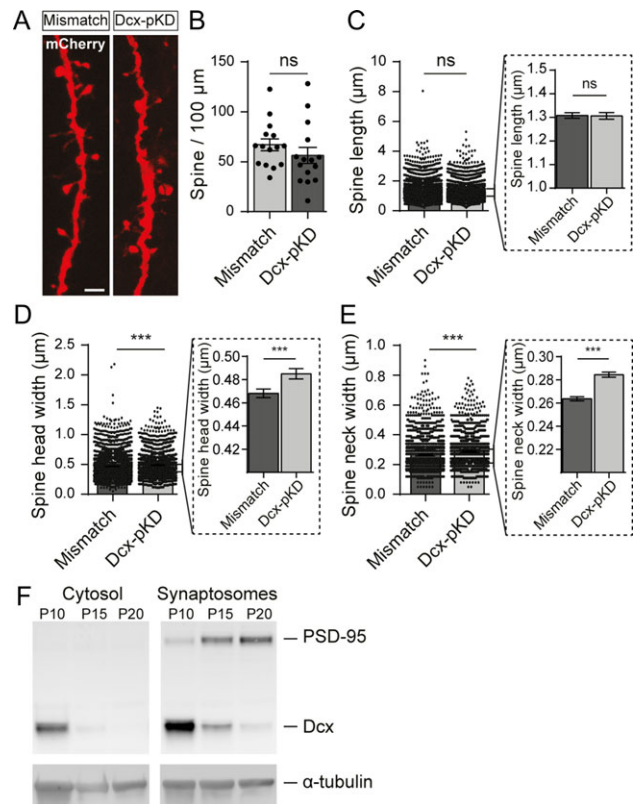

Figure 7. Postnatal knockdown of Dcx slightly increases dendritic spine head and neck widths. (A) High magnification confocal images of dendritic spines from mismatch and Dcx-pKD neurons co-electroporated with mCherry. Scale bar = 2 μm. (B) Quantification of the density of spines for 100 μm of dendrites in mismatch and Dcx-pKD neurons. Values are given as mean ± SEM. Each dot represents a neuron. (C–E) Bar graphs and scatter dot plots illustrating the mean dendritic spine length (C), head width (D) and neck width (E) in mismatch and Dcx-pKD neurons. Values are given as mean ± SEM. Each dot represents a spine. Dotted line frames hold higher magnifications of the initial bar graphs. (D, E) Mann–Whitney test, P-value < 0.001. (F) Western blot of the synaptosomal and cytosolic fractions isolated from cortices of P10, P15, and P20 non-electroporated rats. (Top panels) Detection of PSD-95 (top) and Dcx (bottom). (Bottom panels) Detection of α-tubulin for control.

Next, to further confirm this role, we utilized our postnatal knockdown strategy to silence Dcx during early synaptogenesis without affecting laminar positioning. We compared mIPSCs in Dcx-pKD and mismatch neurons, as we did earlier for mEPSCs. The cumulative frequency curves of mIPSC inter-event intervals were shifted towards higher values suggesting a decreased frequency of mIPSCs in Dcx-pKD neurons as compared with mismatch neurons (Kolmogorov–Smirnov test, P < 0.0001; n = 5769 events from 14 mismatch neurons, 3155 events from 17 Dcx-pKD neurons N = 3–5 animals) (Fig. 9J). This was accompanied by a decreased amplitude and higher half-width of mIPSCs in Dcx-pKD neurons, as indicated by leftward and rightward shifts of cumulative frequency curves respectively (Kolmogorov–Smirnov test, P < 0.0001 for both amplitude and half-width; n = 1122 events from 14 mismatch neurons, 937 events from 13 Dcx-pKD neurons; N = 3–5 animals) (Fig. 9K,L). Together, these electrophysiological differences between mismatch and Dcx-pKD neurons reinforce the notion that Dcx has an influence on GABA synapse formation.

In all, our observations indicate that a correct laminar placement is important for GABAergic synaptogenesis and suggest a role for Dcx in this process.
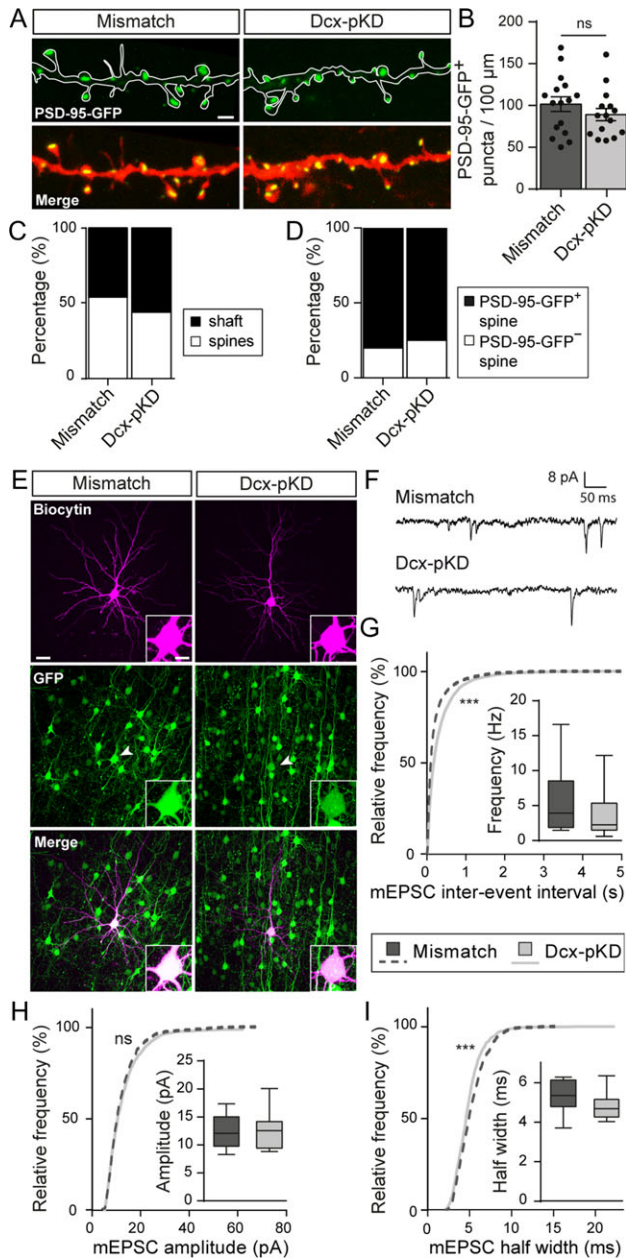
Figure 8. Miniature excitatory currents are impaired after postnatal knockdown of Dcx. (A) High magnification confocal images of mCherry+ dendrites and PSD-95-GFP+ puncta from mismatch and Dcx-pKD neurons. Scale bar = 2 μm. (B) Bar graph and scatter dot plots illustrating the density of PSD-95-GFP+ puncta per 100 μm of dendrites in mismatch and Dcx-pKD neurons. Values are given as mean ± SEM. Each dot represents a neuron. t-test, P-value = 0.2963. (C) Stacked bar graphs showing the relative percentages of PSD-95-GFP+ puncta on dendritic spines and shafts in mismatch and Dcx-pKD neurons. (D) Stacked bar graphs showing the relative percentages of PSD-95-GFP+ and PSD-95-GFP− spines in mismatch and Dcx-pKD neurons. (E) Confocal images of pyramidal neurons filled with biocytin during electrophysiological recordings. Recorded cells were electroporated neurons as indicated by their GFP+ fluorescence (arrow heads). Insets show higher magnification images of the somas. Scale bar = 30 μm/10 μm. (F) Representative traces of mEPSCs recorded from mismatch and Dcx-pKD neurons and analyzed in (G–I). (G–I) Cumulative distributions and box plots of the inter-event interval (G), amplitude (H), and half width (I) values of mEPSCs from mismatch and Dcx-pKD neurons. Box limits indicate the 25th and 75th percentiles; whiskers extend to minimum and maximum values; horizontal lines show the medians. Kolmogorov–Smirnov test, P-value < 0.0001; Mann–Whitney test, (G) P-value = 0.2539, (H) P-value > 0.9999, (I) P-value = 0.1352.

Discussion

In this study, we investigated whether and how laminar misplacement influences the morphological and functional maturation of neocortical neurons. We showed that ectopic positioning impairs the orientation, dendritic growth, spine development and formation of functional glutamatergic and GABAergic synapses in developing neurons. We also highlighted a new role for Dcx in regulating the formation of dendrites and fine-tuning glutamatergic and GABAergic transmission in the cortex. Accordingly, in our model of migration defect induced by Dcx knockdown, the laminar misplacement and Dcx-KD acted synergistically to alter neuronal development. However, since a postnatal knockdown of Dcx induced milder defects, we identified the laminar misplacement as the major contributor to the observed altered neuronal development.

Several rodent models and experimental strategies have been utilized to alter the laminar placement of cortical neurons and study how their maturation is impacted at unusual positions. Most studies, however, were focused on axonal projections and dendritic morphology, and rarely on the development of synapses and spines. Prenatal exposure to ionizing radiations leads to the formation of neuronal masses composed of ectopic neurons born concomitantly to irradiation. Injection of retrograde tracers revealed that these ectopic neurons develop long-distance projections to the spinal cord, as do layer V neurons born at similar gestational ages (D'Amato and Hicks 1980; Jensen and Killackey 1984). In genetic models with subcortical band heterotopia (SBH) similar observations were made, with ectopic neurons developing normal corticospinal and corticothalamic projections (Lee et al. 1997; Bilasy et al. 2009). Heterotopic transplants of embryonic neocortex combined with tracing studies confirmed these findings. Projections sent by neurons grafted at ectopic positions were similar to those of sister neurons sharing the same site of origin (Ebrahimi-Gaillard et al. 1994). Together, these observations suggest that migration of cortical neurons to their fated layers may not be essential for growing axons to reach appropriate targets. On the contrary, neuronal polarity and dendritic outgrowth were both severely affected in the same rodent models. Ectopic neurons in brains prenatally exposed to irradiation or chemicals displayed abnormally oriented apical dendrites (Ferrer et al. 1984; Jensen and Killackey 1984; Sancini et al. 1998; Tschuluun et al. 2005). Randomly oriented apical dendrites were also described in neurons grafted at ectopic locations (Jaeger and Lund 1981). Similarly misoriented neurons were found in genetic models with band heterotopia (Bilasy et al. 2009; Ramos et al. 2016). Last, ectopic neurons displayed various degrees of simplification of dendritic arbors in all models (Jaeger and Lund 1981; Ferrer et al. 1984; Sancini et al. 1998), as well as an apparent reduction of spine density (Tschuluun et al. 2005) in line with our results. Therefore, if axonal development is relatively spared from the consequences of altered laminar placement, our observations confirm that the eventual positioning of neocortical neurons appears instrumental to the subsequent morphogenesis of dendrites, and synapses.

The mechanism responsible for impaired dendritic maturation of ectopic neurons remains to be clarified. Cell-extrinsic mechanisms have been shown to play major roles in dendrite morphogenesis (Valnegri et al. 2015) which can further influence cell-intrinsic mechanisms. Extrinsic cues include numerous secreted factors (Polleux et al. 2000; Joo et al. 2014) and contact-mediated cues (Garrett et al. 2012; Maynard and Stein 2012), as well as neuronal activity (Wong and Ghosh 2002). Ectopic neurons are clearly not exposed to the same
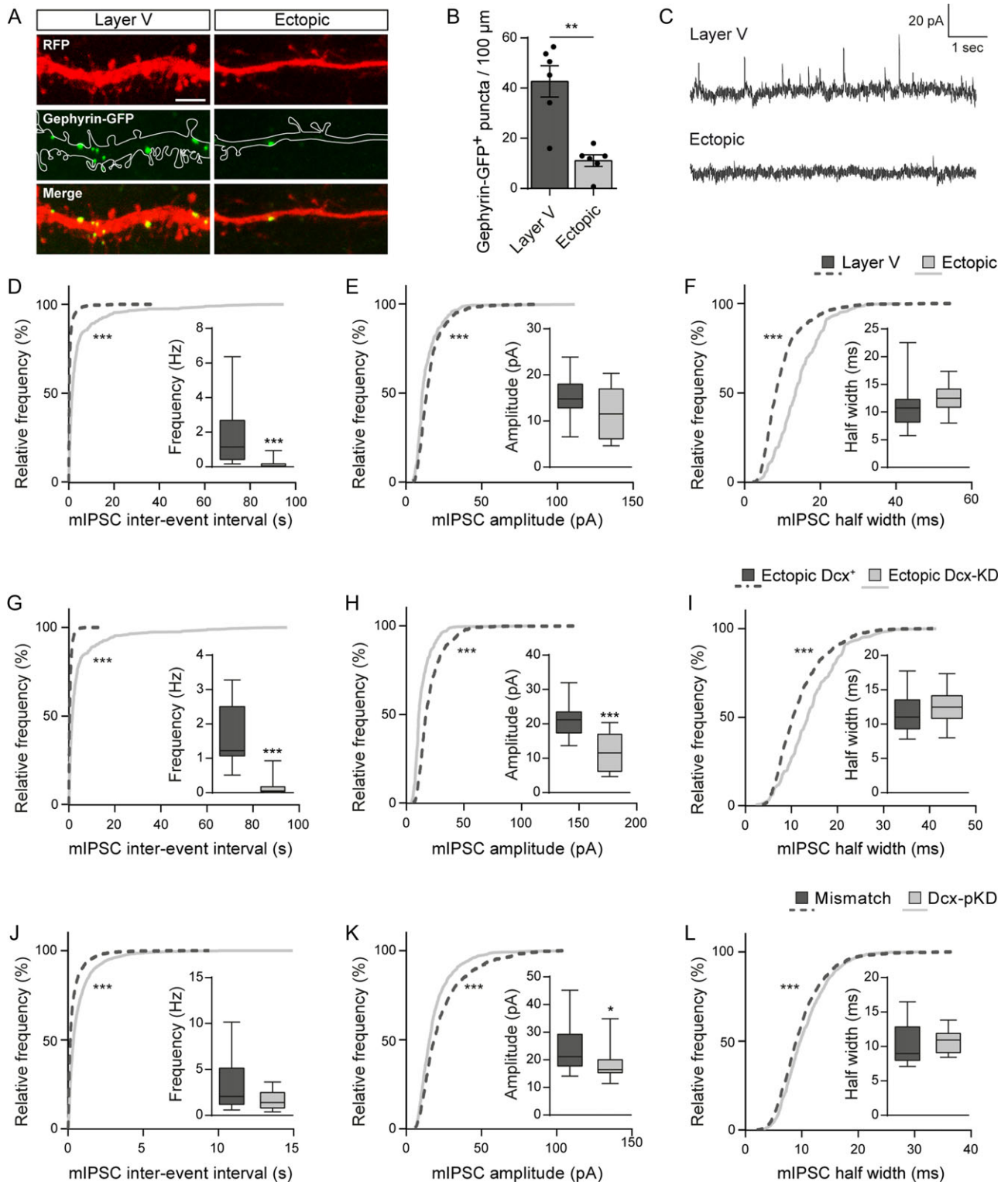
Figure 9. Both laminar positioning and Dcx are important for GABAergic synaptogenesis. (A) Confocal images of RFP[+] dendrites and GFP-gephyrin[+] puncta from layer V and ectopic neurons at P30. Scale bar = 2 μm. (B) Bar graphs and scatter dot plots illustrating the density of GFP-gephyrin[+] puncta per 100 μm of dendrites in layer V and ectopic neurons. Values are given as mean ± SEM. Each dot represents a neuron. Mann–Whitney test, P-value = 0.0043. (C) Representative traces of mIPSCs recorded from layer V and ectopic neurons at P14–15 and analyzed in (D–F). (D–F) Cumulative distributions and box plots of the inter-event interval (D), amplitude (E) and half width (F) values of mIPSCs from layer V and ectopic neurons. Box limits indicate the 25th and 75th percentiles; whiskers extend to minimum and maximum values; horizontal lines show the medians. Kolmogorov–Smirnov test, P-value < 0.0001; Mann–Whitney test, (D) P-value < 0.0001, (E) P-value > 0.9999, (F) P-value = 0.1352. (G–I) Cumulative distributions and box plots of the inter-event interval (G), amplitude (H), and half width (I) values of mIPSCs from ectopic Dcx[+] and ectopic Dcx-KD neurons at P14–15. Box limits indicate the 25th and 75th percentiles; whiskers extend to minimum and maximum values; horizontal lines show the medians. Kolmogorov–Smirnov test, P-value < 0.0001; Mann–Whitney test, (G) P-value < 0.0001, (H) P-value = 0.0004, (I) P-value = 0.4129. (J–L) Cumulative distributions and box plots of the inter-event interval (J), amplitude (K), and half width (L) values of mIPSCs from mismatch and Dcx-pKD neurons at P14–15. Box limits indicate the 25th and 75th percentiles; whiskers extend to minimum and maximum values; horizontal lines show the medians. Kolmogorov–Smirnov test, P-value < 0.0001; Mann–Whitney test, (J) P-value = 0.1021, (K) P-value = 0.0424, (L) P-value = 0.3461.

microenvironment as normally positioned layer V neurons and they may not receive the same inputs as if positioned in layer V, which may influence negatively dendrite development. Recent studies have shown that the development of the dendritic arbors and assembly of excitatory synpases can occur in the absence of glutamatergic neurotransmission (Verhage et al. 2000; Varoqueaux et al. 2002; Bouwman et al. 2004; Lu et al. 2013; Sando et al. 2017; Sigler et al. 2017) even though one of these studies reported that both the dendritic arborization as well as the linear spine densities were reduced in its absence (Sando et al. 2017). A previous study on the Dcx-KD model showed that most ectopic neurons displayed a delayed maturation of GABA-mediated signaling (Ackman et al. 2009). Here, we confirmed and extended these observations. Since early developing GABAergic inputs from cortical interneurons have been shown to control both inhibitory and excitatory synaptogenesis (Oh et al. 2016), defective synaptogenesis in ectopic neurons might result from a defective GABAergic signaling in these neurons.

Our experiments also highlighted a novel role for Dcx in regulating the dendritic and synaptic development of cortical neurons independently of their laminar placement. Both in ectopic and properly placed neurons, knockdown of Dcx leads to a decreased number of dendritic branches when compared with Dcx⁺ neurons in the same position. These results are in line with studies carried out in cultured neurons where Dcx knockdown or mutated forms of human Dcx overexpression resulted in impaired development of the dendritic arbor (Cohen et al. 2008; Blackmore et al. 2010; Yap et al. 2016). Because dendritogenesis relies heavily on microtubules stabilization, Dcx effect could be mediated through its function as a microtubule associated protein (Francis et al. 1999; Horesh et al. 1999; Stiess and Bradke 2011; Moslehi et al. 2017). Indeed, Dcx stabilizes microtubules by linking adjacent protofilaments and counteracting their outward bending in depolymerizing microtubules (Moores et al. 2004, 2006). Moreover, its localization at the distal part of growing neuronal processes places Dcx at a key spot to regulate dendritic branching (Friocourt et al. 2003; Bielas et al. 2007; Bechstedt and Brouhard 2012). Formation of a new dendritic branch can be achieved either through sliding of preassembled microtubules from the soma into the dendrite or through microtubule nucleation, a process leading to de novo polymerization of microtubules (Delandre et al. 2016). Since Dcx has been shown to nucleate microtubules in vitro and in vivo, microtubule nucleation could be the process through which Dcx promotes dendritic ramification of cortical neurons (Horesh et al. 1999; Moores et al. 2004, 2006).

In addition to Dcx involvement in dendritogenesis, we also found a significant enlargement of spine head and neck diameters in Dcx-pKD neurons, suggesting that Dcx acts as a regulator of dendritic spine shape. This finding is in agreement with a previous report identifying Dcx as the downstream effector of Npas4 and Mdm2 which regulate spine formation in newborn neurons of the olfactory bulb (Yoshihara et al. 2014). Spine formation and plasticity rely heavily on the actin cytoskeleton to control spine shape. In developing neurons, Dcx regulates filamentous actin by interacting with neurabin II (spinophilin) thus cross-linking the actin and microtubules cytoskeleton (Tsukada et al. 2003, 2005; Fu et al. 2013). Furthermore, although spines have been considered devoid of microtubules for a long time, several studies have now underlined the presence of dynamic microtubules in these structures (Gu et al. 2008; Hu et al. 2008). Microtubules polymerize transiently into spines and regulate their morphology as well as synaptic plasticity through a cytoskeletal cross-talk with actin (Jaworski

et al. 2009; Merriam et al. 2011, 2013). Because microtubule invasions seem to specifically target spines that are undergoing activity-dependent changes, one hypothesis is that this process helps to regulate synaptic plasticity through molecular cargo transport to the synapse (Schapitz et al. 2010; Dent 2017). Overall, Dcx many interactions with the cytoskeleton are likely to contribute to its regulation of dendritic development, spine morphology and synaptogenesis.

Lastly, our paper identifies laminar misplacement resulting from migration failure as a critical factor holding up the development of cortical neurons. In humans, migration failure during corticogenesis leads to malformations of cortical development that are often associated with epilepsy and intellectual disability (Guerrini and Parrini 2010; Watrin et al. 2015). These symptoms are primarily thought to arise from the structural alterations created by malformations as well as aberrant network connections. However, as these malformations are formed by groups of ectopic neurons, the dendritic and synaptic deficits described above could participate to the etiology of the clinical symptoms. In fact, dendritic shape impairment during development has been linked to lower cognitive capacities later in life (Kulkarni and Firestein 2012; Lin et al. 2017). Moreover, spine alterations and synaptic dysfunctions are well-known mechanisms underlying brain deficits that are known collectively as synaptopathies (Pavlowsky et al. 2012). Finally, since Dcx also seems to regulate some aspects of neuronal development, this study may be relevant for a migration disorder arising from Dcx mutations, called SBH (Barkovich et al. 1994; Gleeson et al. 1998; des Portes et al. 1998; Tanaka and Gleeson 2008; Bahi-Buisson et al. 2013). Patients with SBH suffer from drug-resistant epilepsy and intellectual disability. According to our results, laminar misplacement and Dcx deficiency could contribute to the pathophysiology of SBH by acting synergistically to alter the maturation of ectopic neurons.

Supplementary Material

Supplementary material is available at *Cerebral Cortex* online.

Authors' Contributions

F.S.M., F.W., J.B.M., and A.R. designed and conceived the experiments. E.B. and F.S. performed in utero electroporations. L.F. and F.W. performed the cloning and preparation of plasmids. H.K provided the PSD-95-GFP and GFP-gephyrin plasmids. F.W. prepared the synaptosomes and performed the Western blot analyses. F.S.M. and F.W. performed morphological analyses. G. C. and F.W. performed electron microscopy experiments. V.P. and S.S. performed electrophysiological experiments. F.S.M., S. S, V.P., F.W., A.R., and J.B.M. analyzed the data. F.S.M., F.W., A. R., and J.B.M. wrote the article.

Funding

Notes

Materials & Correspondence

Correspondence and requests for materials should be addressed to F.W. (email: francoise.watrin@inserm.fr) and J.B.M. (jean-bernard.manent@inserm.fr).

References

Ackman JB, Aniksztejn L, Crepel V, Becq H, Pellegrino C, Cardoso C, Ben-Ari Y, Represa A. 2009. Abnormal network activity in a targeted genetic model of human double cortex. J Neurosci. 29:313–327.

Ako R, Wakimoto M, Ebisu H, Tanno K, Hira R, Kasai H, Matsuzaki M, Kawasaki H. 2011. Simultaneous visualization of multiple neuronal properties with single-cell resolution in the living rodent brain. Mol Cell Neurosci. 48:246–257.

Auladell C, Martinez A, Alcantara S, Super H, Soriano E. 1995. Migrating neurons in the developing cerebral cortex of the mouse send callosal axons. Neuroscience. 64:1091–1103.

Baek ST, Kerjan G, Bielas SL, Lee JE, Fenstermaker AG, Novarino G, Gleeson JG. 2014. Off-target effect of doublecortin family shRNA on neuronal migration associated with endogenous microRNA dysregulation. Neuron. 82:1255–1262.

Bahi-Buisson N, Souville I, Fourniol FJ, Toussaint A, Moores CA, Houdusse A, Lemaitre JY, Poirier K, Khalaf-Nazzal R, Hully M, et al. 2013. New insights into genotype-phenotype correlations for the doublecortin-related lissencephaly spectrum. Brain. 136:223–244.

Bai J, Ramos RL, Ackman JB, Thomas AM, Lee RV, LoTurco JJ. 2003. RNAi reveals doublecortin is required for radial migration in rat neocortex. Nat Neurosci. 6:1277–1283.

Barkovich AJ, Guerrini R, Battaglia G, Kalifa G, N'Guyen T, Parmeggiani A, Santucci M, Giovanardi-Rossi P, Granata T, D'Incerti L. 1994. Band heterotopia: correlation of outcome with magnetic resonance imaging parameters. Ann Neurol. 36:609–617.

Bechstedt S, Brouhard GJ. 2012. Doublecortin recognizes the 13-protofilament microtubule cooperatively and tracks microtubule ends. Dev Cell. 23:181–192.

Berry KP, Nedivi E. 2017. Spine dynamics: are they all the same? Neuron. 96(1):43–55.

Bielas SL, Serneo FF, Chechlacz M, Deerinck TJ, Perkins GA, Allen PB, Ellisman MH, Gleeson JG. 2007. Spinophilin facilitates dephosphorylation of doublecortin by PP1 to mediate microtubule bundling at the axonal wrist. Cell. 129:579–591.

Bilasy SE, Satoh T, Ueda S, Wei P, Kanemura H, Aiba A, Terashima T, Kataoka T. 2009. Dorsal telencephalon-specific RA-GEF-1 knockout mice develop heterotopic cortical mass and commissural fiber defect. Eur J Neurosci. 29:1994–2008.

Blackmore MG, Moore DL, Smith RP, Goldberg JL, Bixby JL, Lemmon VP. 2010. High content screening of cortical neurons identifies novel regulators of axon growth. Mol Cell Neurosci. 44:43–54.

Bouwman J, Maia AS, Camoletto PG, Posthuma G, Roubos EW, Oorschot VMJ, Klumperman J, Verhage M. 2004. Quantification of synapse formation and maintenance in vivo in the absence of synaptic release. Neuroscience. 126:115–126.

Cohen D, Segal M, Reiner O. 2008. Doublecortin supports the development of dendritic arbors in primary hippocampal neurons. Dev Neurosci. 30:187–199.

Danielson E, Lee SH. 2014. SynPAnal: software for rapid quantification of the density and intensity of protein puncta from fluorescence microscopy images of neurons. PLoS One. 9: e115298.

Delandre C, Amikura R, Moore AW. 2016. Microtubule nucleation and organization in dendrites. Cell Cycle. 15: 1685–1692.

Dent EW. 2017. Of microtubules and memory: implications for microtubule dynamics in dendrites and spines. Mol Biol Cell. 28:1–8.

des Portes V, Francis F, Pinard JM, Desguerre I, Moutard ML, Snoeck I, Meiners LC, Capron F, Cusmai R, Ricci S, et al. 1998. doublecortin is the major gene causing X-linked subcortical laminar heterotopia (SCLH). Hum Mol Genet. 7: 1063–1070.

Desikan RS, Barkovich AJ. 2016. Malformations of cortical development. Ann Neurol. 80:797–810.

D'Amato CJ, Hicks SP. 1980. Development of the motor system: effects of radiation on developing corticospinal neurons and locomotor function. Exp Neurol. 70:1–23.

Ebrahimi-Gaillard A, Guitet J, Garnier C, Roger M. 1994. Topographic distribution of efferent fibers originating from homotopic or heterotopic transplants: heterotopically transplanted neurons retain some of the developmental characteristics corresponding to their site of origin. Brain Res Dev Brain Res. 77:271–283.

Ferrer I, Xumetra A, Santamaria J. 1984. Cerebral malformation induced by prenatal X-irradiation: an autoradiographic and Golgi study. J Anat. 138(Pt 1):81–93.

Francis F, Koulakoff A, Boucher D, Chafey P, Schaar B, Vinet MC, Friocourt G, McDonnell N, Reiner O, Kahn A, et al. 1999. Doublecortin is a developmentally regulated, microtubule-associated protein expressed in migrating and differentiating neurons. Neuron. 23:247–256.

Friocourt G, Koulakoff A, Chafey P, Boucher D, Fauchereau F, Chelly J, Francis F. 2003. Doublecortin functions at the extremities of growing neuronal processes. Cereb Cortex. 13: 620–626.

Fu X, Brown KJ, Yap CC, Winckler B, Jaiswal JK, Liu JS. 2013. Doublecortin (Dcx) family proteins regulate filamentous actin structure in developing neurons. J Neurosci. 33:709–721.

Garrett AM, Schreiner D, Lobas MA, Weiner JA. 2012. Gamma-protocadherins control cortical dendrite arborization by regulating the activity of a FAK/PKC/MARCKS signaling pathway. Neuron. 74:269–276.

Gleeson JG, Allen KM, Fox JW, Lamperti ED, Berkovic S, Scheffer I, Cooper EC, Dobyns WB, Minnerath SR, Ross ME, et al. 1998. Doublecortin, a brain-specific gene mutated in human X-linked lissencephaly and double cortex syndrome, encodes a putative signaling protein. Cell. 92:63–72.

Gonzalez-Lozano MA, Klemmer P, Gebuis T, Hassan C, van Nierop P, van Kesteren RE, Smit AB, Li KW. 2016. Dynamics

of the mouse brain cortical synaptic proteome during post-natal brain development. Sci Rep. 6:35456.

Gu J, Firestein BL, Zheng JQ. 2008. Microtubules in dendritic spine development. J Neurosci. 28:12120–12124.

Guerrini R, Dobyns WB. 2014. Malformations of cortical development: clinical features and genetic causes. Lancet Neurol. 13:710–726.

Guerrini R, Parrini E. 2010. Neuronal migration disorders. Neurobiol Dis. 38:154–166.

Hatanaka Y, Murakami F. 2002. In vitro analysis of the origin, migratory behavior, and maturation of cortical pyramidal cells. J Comp Neurol. 454:1–14.

Horesh D, Sapir T, Francis F, Wolf SG, Caspi M, Elbaum M, Chelly J, Reiner O. 1999. Doublecortin, a stabilizer of microtubules. Hum Mol Genet. 8:1599–1610.

Hu X, Viesselmann C, Nam S, Merriam E, Dent EW. 2008. Activity-dependent dynamic microtubule invasion of dendritic spines. J Neurosci. 28:13094–13105.

Jaeger CB, Lund RD. 1981. Transplantation of embryonic occipital cortex to the brain of newborn rats: a Golgi study of mature and developing transplants. J Comp Neurol. 200: 213–230.

Jaworski J, Kapitein LC, Gouveia SM, Dortland BR, Wulf PS, Grigoriev I, Camera P, Spangler SA, Di Stefano P, Demmers J, et al. 2009. Dynamic microtubules regulate dendritic spine morphology and synaptic plasticity. Neuron. 61:85–100.

Jensen KF, Killackey HP. 1984. Subcortical projections from ectopic neocortical neurons. Proc Natl Acad Sci U S A. 81: 964–968.

Joo W, Hippenmeyer S, Luo L. 2014. Dendrite morphogenesis depends on relative levels of NT-3/TrkC signaling. Science. 346:626–629.

Kulkarni VA, Firestein BL. 2012. The dendritic tree and brain disorders. Mol Cell Neurosci. 50:10–20.

Lee KS, Schottler F, Collins JL, Lanzino G, Couture D, Rao A, Hiramatsu K, Goto Y, Hong SC, Caner H, et al. 1997. A genetic animal model of human neocortical heterotopia associated with seizures. J Neurosci. 17:6236–6242.

Lin Q, Ponnusamy R, Widagdo J, Choi JA, Ge W, Probst C, Buckley T, Lou M, Bredy TW, Fanselow MS, et al. 2017. MicroRNA-mediated disruption of dendritogenesis during a critical period of development influences cognitive capacity later in life. Proc Natl Acad Sci U S A. 114:9188–9193.

Lu W, Bushong EA, Shih TP, Ellisman MH, Nicoll RA. 2013. The cell-autonomous role of excitatory synaptic transmission in the regulation of neuronal structure and function. Neuron. 78:433–439.

Maynard KR, Stein E. 2012. DSCAM contributes to dendrite arborization and spine formation in the developing cerebral cortex. J Neurosci. 32:16637–16650.

Merriam EB, Lumbard DC, Viesselmann C, Ballweg J, Stevenson M, Pietila L, Hu X, Dent EW. 2011. Dynamic microtubules promote synaptic NMDA receptor-dependent spine enlargement. PLoS One. 6:e27688.

Merriam EB, Millette M, Lumbard DC, Saengsawang W, Fothergill T, Hu X, Ferhat L, Dent EW. 2013. Synaptic regulation of microtubule dynamics in dendritic spines by calcium, F-actin, and drebrin. J Neurosci. 33:16471–16482.

Moczulska KE, Pichler P, Schutzbier M, Schleiffer A, Rumpel S, Mechtler K. 2014. Deep and precise quantification of the mouse synaptosomal proteome reveals substantial remodeling during postnatal maturation. J Proteome Res. 13:4310–4324.

Moores CA, Perderiset M, Francis F, Chelly J, Houdusse A, Milligan RA. 2004. Mechanism of microtubule stabilization by doublecortin. Mol Cell. 14:833–839.

Moores CA, Perderiset M, Kappeler C, Kain S, Drummond D, Perkins SJ, Chelly J, Cross R, Houdusse A, Francis F. 2006. Distinct roles of doublecortin modulating the microtubule cytoskeleton. EMBO J. 25:4448–4457.

Moslehi M, Ng DCH, Bogoyevitch MA. 2017. Dynamic microtubule association of Doublecortin X (DCX) is regulated by its C-terminus. Sci Rep. 7:5245.

Noctor SC, Martinez-Cerdeno V, Ivic L, Kriegstein AR. 2004. Cortical neurons arise in symmetric and asymmetric division zones and migrate through specific phases. Nat Neurosci. 7:136–144.

Oh WC, Lutzu S, Castillo PE, Kwon H. 2016. De novo synaptogenesis induced by GABA in the developing mouse cortex. Science. 353:1037–1040.

Pavlowsky A, Chelly J, Billuart P. 2012. Emerging major synaptic signaling pathways involved in intellectual disability. Mol Psychiatry. 17:682–693.

Petit LF, Jalabert M, Buhler E, Malvache A, Peret A, Chauvin Y, Watrin F, Represa A, Manent JB. 2014. Normotopic cortex is the major contributor to epilepsy in experimental double cortex. Ann Neurol. 76:428–442.

Polleux F, Morrow T, Ghosh A. 2000. Semaphorin 3A is a chemoattractant for cortical apical dendrites. Nature. 404: 567–573.

Ramos RL, Toia AR, Pasternack DM, Dotzler TP, Cuoco JA, Esposito AW, Le MM, Parker AK, Goodman JH, Sarkisian MR. 2016. Neuroanatomical characterization of the cellular and axonal architecture of subcortical band heterotopia in the BXD29-Tlr4lps-2J/J mouse cortex. Neuroscience. 337:48–65.

Sancini G, Franceschetti S, Battaglia G, Colacitti C, Di Luca M, Spreafico R, Avanzini G. 1998. Dysplastic neocortex and subcortical heterotopias in methylazoxymethanol-treated rats: an intracellular study of identified pyramidal neurones. Neurosci Lett. 246:181–185.

Sando R, Bushong E, Zhu Y, Huang M, Considine C, Phan S, Ju S, Uytiepo M, Ellisman M, Maximov A. 2017. Assembly of excitatory synapses in the absence of glutamatergic neurotransmission. Neuron. 94:312–321.e3.

Schapitz IU, Behrend B, Pechmann Y, Lappe-Siefke C, Kneussel SJ, Wallace KE, Stempel AV, Buck F, Grant SGN, Schweizer M, et al. 2010. Neuroligin 1 is dynamically exchanged at postsynaptic sites. J Neurosci. 30:12733–12744.

Schindelin J, Arganda-Carreras I, Frise E, Kaynig V, Longair M, Pietzsch T, Preibisch S, Rueden C, Saalfeld S, Schmid B, et al. 2012. Fiji: an open-source platform for biological-image analysis. Nat Methods. 9:676–682.

Schwartz ML, Rakic P, Goldman-Rakic PS. 1991. Early phenotype expression of cortical neurons: evidence that a subclass of migrating neurons have callosal axons. Proc Natl Acad Sci U S A. 88:1354–1358.

Scorcioni R, Polavaram S, Ascoli GA. 2008. L-Measure: a web-accessible tool for the analysis, comparison and search of digital reconstructions of neuronal morphologies. Nat Protoc. 3:866–876.

Sigler A, Oh WC, Imig C, Altas B, Kawabe H, Cooper BH, Kwon H, Rhee J, Brose N. 2017. Formation and maintenance of functional spines in the absence of presynaptic glutamate release. Neuron. 94:304–311.e4.

Stiess M, Bradke F. 2011. Neuronal polarization: the cytoskeleton leads the way. Dev Neurobiol. 71:430–444.

Tabata H, Nakajima K. 2001. Efficient in utero gene transfer system to the developing mouse brain using electroporation: visualization of neuronal migration in the developing cortex. Neuroscience. 103:865–872.

Tanaka T, Gleeson JG. 2008. Subcortical laminar (band) heterotopia. Handb Clin Neurol. 87:191–204.

Tschuluun N, Wenzel JH, Katleba K, Schwartzkroin PA. 2005. Initiation and spread of epileptiform discharges in the methylazoxymethanol acetate rat model of cortical dysplasia: functional and structural connectivity between CA1 heterotopia and hippocampus/neocortex. Neuroscience. 133:327–342.

Tsukada M, Prokscha A, Oldekamp J, Eichele G. 2003. Identification of neurabin II as a novel doublecortin interacting protein. Mech Dev. 120:1033–1043.

Tsukada M, Prokscha A, Ungewickell E, Eichele G. 2005. Doublecortin association with actin filaments is regulated by neurabin II. J Biol Chem. 280:11361–11368.

Valnegri P, Puram SV, Bonni A. 2015. Regulation of dendrite morphogenesis by extrinsic cues. Trends Neurosci. 38:439–447.

Varoqueaux F, Sigler A, Rhee J, Brose N, Enk C, Reim K, Rosenmund C. 2002. Total arrest of spontaneous and evoked synaptic transmission but normal synaptogenesis in the absence of Munc13-mediated vesicle priming. Proc Natl Acad Sci U S A. 99:9037–9042.

Verhage M, Maia AS, Plomp JJ, Brussaard AB, Heeroma JH, Vermeer H, Toonen RF, Hammer RE, van den Berg TK, Missler M, et al. 2000. Synaptic assembly of the brain in the absence of neurotransmitter secretion. Science. 287:864–869.

Watrin F, Manent JB, Cardoso C, Represa A. 2015. Causes and consequences of gray matter heterotopia. CNS Neurosci Ther. 21:112–122.

Wong ROL, Ghosh A. 2002. Activity-dependent regulation of dendritic growth and patterning. Nat Rev Neurosci. 3: 803–812.

Yap CC, Digilio L, McMahon L, Roszkowska M, Bott CJ, Kruczek K, Winckler B. 2016. Different Doublecortin (DCX) patient alleles show distinct phenotypes in cultured neurons: evidence for divergent loss-of-function and "off-pathway" cellular mechanisms. J Biol Chem. 291:26613–26626.

Yoshihara S, Takahashi H, Nishimura N, Kinoshita M, Asahina R, Kitsuki M, Tatsumi K, Furukawa-Hibi Y, Hirai H, Nagai T, et al. 2014. Npas4 regulates Mdm2 and thus Dcx in experience-dependent dendritic spine development of newborn olfactory bulb interneurons. Cell Rep. 8:843–857.